


Article

# Numerical Investigation of Strength Mismatch Effect on Ductile Crack Growth Resistance in Welding Pipe

Lin Su <sup>1</sup>, Jie Xu <sup>2</sup>, Wei Song <sup>3,\*</sup> , Lingyu Chu <sup>2</sup>, Hanlin Gao <sup>2</sup>, Pengpeng Li <sup>2</sup> and Filippo Berto <sup>4,\*</sup><sup>1</sup> SINOPEC Oil & Gas Pipeline Inspection Co., Ltd., Xuzhou 221008, China; sul.gdcy@sinopec.com<sup>2</sup> School of Materials Science and Physics, China University of Mining and Technology (CUMT), Xuzhou 221116, China; j.xu@cumt.edu.cn (J.X.); chulingyu0zi@163.com (L.C.); TS19180050P31@cumt.edu.cn (H.G.); lpp0424@yeah.net (P.L.)<sup>3</sup> School of Mechanical & Electrical Engineering, Xuzhou University of Technology, Xuzhou 221018, China<sup>4</sup> Department of Mechanical and Industrial Engineering, Norwegian University of Science and Technology (NTNU), 7491 Trondheim, Norway

\* Correspondence: songwei@xuzit.edu.cn (W.S.); filippo.berto@ntnu.no (F.B.); Tel.: +86-152-0450-6099 (W.S.)

Received: 21 November 2019; Accepted: 27 January 2020; Published: 18 February 2020



**Abstract:** The effect of strength mismatch (ratio between the yield stress of weld metal and base metal,  $M_y$ ) on the ductile crack growth resistance of welding pipe was numerically analyzed. The ductile fracture behavior of welding pipe was determined while using the single edge notched bending (SENB) and single edge notched tension (SENT) specimens, as well as axisymmetric models of circumferentially cracked pipes for comparison. Crack growth resistance curves (as denoted by crack tip opening displacement-resistance (CTOD-R curve) have been computed using the complete Gurson model. A so-called CTOD- $Q$ - $M$  formulation was proposed to calculate the weld mismatch constraint  $M$ . It has been shown that the fracture resistance curves significantly increase with the increase of the mismatch ratio. As for SENT and pipe, the larger  $M_y$  causes the lower mismatch constraint  $M$ , which leads to the higher fracture toughness and crack growth resistance curves. When compared with the standard SENB, the SENT specimen and the cracked pipe have a more similar fracture resistance behavior. The results present grounds for justification of usage of SENT specimens in fracture assessment of welding cracked pipes as an alternative to the traditional conservative SENB specimens.

**Keywords:** weld strength mismatch; ductile tearing; pipelines; mismatch constraint

## 1. Introduction

The original idea of application of conventional fracture mechanics was that a single parameter, such as crack tip opening displacement (CTOD) and  $J$ -integral, could well characterize the crack-tip stress field. Additionally, the unique fracture resistance curve,  $J$ -R or CTOD-R, was enough to reflect the material behavior. The shortages of such idealized one-parameter theory, however, become increasingly clear by studying the diversified crack-tip fields [1–3]. Thus, two-parameter fracture theory (i.e., elastic  $T$ -stress [4] and  $J$ - $Q$  theory [5,6]) has been developed to characterize the crack-tip stress field and measure the constraint levels for various geometries and loading configurations in elastic-plastic materials.

Crack-like defects always produce during in-service operation or fabrication for pipelines. The single edge notched bending (SENB) specimen is usually treated as an experimental standard. While the researches make it clear that the standard SENB has certain conservatism due to its remarkably higher geometry constraint than actual pipes with circumferential surface cracks. The single edge notched tension (SENT) specimen has been frequently suggested for its more similar geometry constraint as the cracks in pipes in front of the crack tip [7–10].

Weldments commonly exist in engineering structures and they tend to be the most critical part of welded structures for the instability of fracture. Weld strength mismatch plays a crucial role in structural integrity assessment. For this known reason, researches focused on characterizing the local stress fields of weldment and heat affected zone (HAZ) [11–13] were carried out in recent decades. For such a mismatched weldment, there are two types of constraints consisting of geometric constraint induced by specimen dimensions, loading modes and crack size, and the material constraint induced by inhomogeneous material properties [14,15]. Zhang et al. [14] proposed the mismatch constraint parameter  $M$  to describe the influence of material mismatch on the crack tip stress field. Furthermore, a so-called  $J$ - $Q$ - $M$  theory (see e.g., Zhang et al. [14,16,17]), where both constraint effects were considered to characterize the local stress field near the crack tip was developed by SINTEF/NTNU. Recently, Zerbst reviewed the fracture results of inhomogeneous microstructure for materials testing and failure assessment [18]. The Claudio Ruggieri group examined the effect of weld strength mismatch and crack sizes ( $a/W$  ratios) on  $J$  and CTOD ductile fracture parameters while using SENT specimens based on plastic  $\eta$ -factors and load separation analysis [19,20]. On the other hand, the similar investigation about strength mismatch effect on fracture mechanical behavior for SA 508-Alloy 52 narrow gap dissimilar metal weld was conducted by microstructural and fracture resistance characterizations [21]. The results showed that the mismatch state caused the crack to propagate towards the fusion boundary. When the crack initiated from HAZ, the crack propagation occurred towards the weld zone for the undermatched condition [22]. Recently, Qiang Bin et al. studied ductile crack growth behaviors at different locations of a weld joint for an X80 pipeline steel by experimental and numerical methods, it demonstrated that the Gurson-Tvergaard-Needleman (GTN) model can differentiate the constraint conditions and predict the  $J$ - $R$  curves at different joint locations for SENB and SENT specimens accurately [23].

There are no reported studies so far on the ductile fracture resistance behavior for strength-mismatched welding pipe under large scale yielding conditions to the best of our knowledge. Thus, present work mainly investigates the effects of specimen geometry and weld strength mismatch on the ductile fracture resistance of welding pipe. Additionally, the constraint state ahead of a propagating crack is taken into account. The traditionally used deep-cracked SENB (with  $a/W = 0.5$ ) specimen and the shallow and deep-cracked SENT (with  $a/W = 0.2$  and  $0.5$ ) specimens as well as the axisymmetric models for pipes with internal circumferential cracks are selected for comparison in order to characterize the crack tip constraint effect on the fracture toughness. In present work, only a bi-material central crack (namely, the heat affected zone is neglected and crack is located in the center of weld metal that is besieged by base metal) is considered. Additionally, the tri-material and interface crack problem will be discussed in another manuscript.

## 2. Background and Numerical Procedures

### 2.1. Background and Numerical Procedures

It has been well known that the nucleation, growth, and coalescence of microvoids lead to the ductile crack growth in metals. In recent decades, large amounts of investigations for elastic-plastic materials incorporating void mechanisms have been made in developing the constitutive models and the widely accepted one seems to be the Gurson-Tvergaard-Needleman (GTN) model, which is firstly introduced by Gurson [24] and then modified by Tvergaard and Needleman [25–27]. The yield function of the GTN model keeps to the following form:

$$\varphi(\sigma_{ij}, f^*, \sigma_y) = \frac{\sigma_e^2}{\sigma_y^2} + 2q_1 f^* \cosh\left(\frac{3q_2 \sigma_m}{2\sigma_y}\right) - 1 - q_1 f^{*2} \quad (1)$$

in which  $\sigma_y$  is the flow stress of the matrix material, and  $f^*$  is the effective void volume fraction,  $\sigma_e$  is the von Mises stress, and  $\sigma_m$  is the mean normal stress component. Constants  $q_1$  and  $q_2$ , as introduced by Tvergaard, were used to modify the Gurson model.

Introduced by Tvergaard and Needleman,  $f^*$  follows the next form:

$$\begin{aligned} f^* &= f & f \leq f_c \\ f^* &= f_c + \frac{f_u^* - f_c}{f_F - f_c} (f - f_c) & f > f_c \end{aligned} \quad (2)$$

where  $f_u^* = 1/q_1$ . In Equation (2),  $f$  represents the void volume,  $f_c$  (the so-called critical void volume fraction criterion) assumes that the void coalescence occurs, and  $f_F$  is the void volume fraction at final failure.

Combining Thomason's plastic limit load model [28] and the GTN model, Zhang et al. [29] proposed a so-called "complete Gurson model (CGM)". It should be clear that, in the CGM, an automatically determined  $f_c$  was around 2%, and  $f_F = 0.20 + 2f_0$ . In this paper,  $q_1 = 1.5$ ,  $q_2 = 1.0$  and  $q_3 = q_1^2$  are applied to the GTN model and  $f_0 = 0.001$  for all analyses have been considered. By using a user material subroutine UMAT that was developed by Zhang [30–32], the complete Gurson model was implemented in Abaqus.

## 2.2. Crack Tip Constraint

It is well known that a combination of geometry constraint [4,5], material mismatch constraint [14,15], prestrain history [33], and welding residual stresses constraint [34,35] affects the crack tip stress field, which makes fracture toughness is no longer a material constant. The purpose of studying constraint is to find an appropriate parameter(s) to characterize the crack tip stress-strain fields and achieve the goal that the result of fracture toughness can be transferred from one test geometry to the others. In the following, only the constraints due to geometry and material mismatch are briefly reviewed.

### 2.2.1. Geometrical Constraint J-Q Formulation

For homogeneous materials, the single-parameter based approach has a limited range of validity. The crack tip stress field is not completely controlled by  $J$  or CTOD, which is also influenced by specimen dimensions, initial crack size, as well as loading mode. As proposed by Betegon and Hancock [4],  $J$ - $T$  theory is mainly used to depict the crack tip stress field of elastic material. For elastic-plastic fracture problems, Shih and O'Dowd'  $J$ - $Q$  formulation [5,6] and Yang and Chao'  $J$ - $A_2$  [36] formulation represent the influence of geometry constraint on the fracture toughness, in which  $J$  sets the deformation level and the  $Q$  and  $A_2$  parameters are a direct measurement of the level of the elastic-plastic stress-fields. It has been shown that the  $Q$  parameter and elastic  $T$  stress are uniquely linked in finite geometries under small-scale yielding [5,6]. Under large-scale yielding conditions, because of the interaction of the plastic zone with the specimen boundaries, the one to one relationship loses. The  $J$ - $Q$  theory can be written as:

$$\sigma_{ij} = \sigma_{ij}^{HRR} + Q\sigma_0 \left( \frac{r}{J/\sigma_0} \right)^q \hat{\sigma}_{ij}(\theta, n) \quad (3)$$

where  $\sigma_{ij}^{HRR}$  is the  $J$ -controlled Hutchinson Rice Rosengren (HRR) stress field,  $\sigma_0$  is yield stress,  $\theta$  and  $r$  represent the polar coordinates centered at the crack tip,  $n$  is the hardening exponent. In the range of  $1 < r/(J/\sigma_0) < 5$ , they found that  $|q| \ll 1$  and for  $|\theta| < \pi/2$ ,  $\hat{\sigma}_{ij}(r, \theta) \approx \text{constant}$  for  $i = j$  and  $\hat{\sigma}_{ij}(r, \theta) \approx 0$  for  $i \neq j$ .

### 2.2.2. Material Mismatch-Induced Constraint J-Q-M Formulation

There is often a mismatch between the base metal and the weld metal for the nature of materials. For such a mismatched weldment, the crack tip stress field is influenced by the geometric constraint and the strength mismatch that is induced by the inhomogeneous material properties [14,15]. Zhang et al. defined a constraint parameter  $M$  [14] to describe the effect of material mismatch on the crack tip stress field. They also found that geometric constraint shifts the near-tip stress level up and down with negligibly affecting the material mismatch constraint parameter  $M$ , which indicates that  $Q$  has

little connection with  $M$ . Afterwards, on the base of these findings, a so-called  $J$ - $Q$ - $M$  formulation was presented:

$$\sigma_{ij} \approx \sigma_{ij}^{M=0, T=0} + Q\sigma_0\delta_{ij} + M\sigma_0f_{ij}(\theta + 12\beta, n) \tag{4}$$

where the  $Q$  parameter is used to rank the effect of geometry constraint on the crack-tip constraint. Additionally, the  $M$  value describes the material mismatch. In the former formula,  $n$  and  $\sigma_0$  are the hardening exponent and yield stress of the reference material,  $f_{ij}$  represents the angular function, which only depends on the reference material,  $\beta = 1$  for under-match and  $\beta = 0$  for over match and even match [14]. Equation (4) applies to the mismatch and reference materials, and it is much fitter for the later.

In this study, the CTOD was used as the fracture parameter. Shih [37] has shown that the  $J$  and CTOD, for a given elastic-plastic material, are uniquely linked. Nevertheless, it is advantageous to calculate the crack driving force. The crack tip stress field with and without strength mismatch can be written in terms of CTOD:

$$\begin{aligned} \sigma_{ij}^{My=1.0} &= \sigma_{ij}^{Ref} + Q\sigma_0\delta_{ij} \\ \sigma_{ij}^{My\neq 1.0} &= \sigma_{ij}^{My=1.0} + \Delta\sigma_{ij}^M \end{aligned} \tag{5}$$

where  $\Delta\sigma_{ij}^M$  denotes the difference between stress fields that are caused by the strength mismatch. The reference solution  $\sigma_{ij}^{Ref}$  can be obtained from the HRR solution or a modified boundary layer (MBL) model under small-scale yielding. In the current work, the MBL with  $T = 0$  was used. Mismatch ratio  $M_y$  was defined as  $M_y = \sigma_{ys}^{WM}/\sigma_{ys}^{BM}$ , where  $\sigma_{ys}^{WM}$  and  $\sigma_{ys}^{BM}$  represent the yield stress of the weld metal and base metal.

The following definition of  $Q$  and  $M$  has been obtained because of the use of CTOD as crack driving force [5,6,14], according to the former formulas:

$$\begin{aligned} Q &= \frac{\sigma_{ij} - \sigma_{ij}^{Ref}}{\sigma_0} = \frac{\sigma_{22} - \sigma_{22}^{Ref}}{\sigma_0} \\ M &= \frac{\Delta\sigma_{ij}^M}{\sigma_0} = \frac{\sigma_{22}^{My\neq 1.0} - \sigma_{22}^{My=1.0}}{\sigma_0} \end{aligned} , \theta = 0, \quad 1 \leq \frac{r}{\delta} \leq 5 \tag{6}$$

where  $\sigma_{ij}$  is the opening stress component of interest,  $\sigma_{ij}^{Ref}$  is the reference stress component that was obtained by MBL model solution with  $T = 0$ ,  $r$  is the distance from the crack tip along the crack plane. Additionally, in present work, the focus is placed on the stress field ( $\sigma_{22}$ ) perpendicular to the direction of crack growth at the crack front ( $\theta = 0, r/\delta = 3$ ).

### 2.3. Material

For the base metal studied in this study, the uniaxial stress-strain curve follows the power-law hardening rule:

$$\sigma_f = \sigma_0 \left( 1 + \frac{\epsilon_p}{\epsilon_0} \right)^n \tag{7}$$

where  $\sigma_f$  is the flow stress, the yield stress  $\sigma_0$  is 733 MPa,  $\epsilon_p$  is the equivalent plastic strain,  $\epsilon_0 = \sigma_0/E$  is the yield strain, Young's modulus  $E$  is 200 GPa, the Poisson's ratio  $\nu$  is 0.3, and  $n = 0.05$  is the plastic strain hardening exponent. The yield stress value for this material considered herein represents typically high strength pipeline steels, such as API X100 grade steels.

The weld material flow properties in finite element analyses covered the following strength mismatch levels: 10%, 20% under match [ $M_y = 0.8, 0.9$ ], even match [ $M_y = 1.0$ ] and 10%, 30% over match [ $M_y = 1.1, 1.3$ ]. The welding structure is modeled as a bi-material system (the HAZ is not taken into account), with yield stress and hardening properties of the base metal adopted as fixed in all of the analyses. Figure 1 shows the true stress-strain curves for materials with various strength mismatch ratios  $M_y$ .

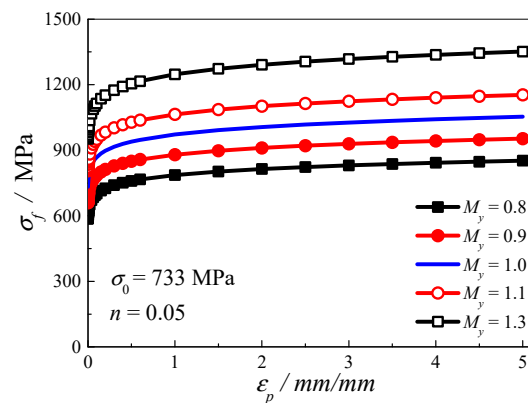


**Figure 1.** The true stress-strain curve of weld material with different strength mismatch ratios.

## 2.4. The Finite Element Models

### 2.4.1. The SENB and SENT Specimens

The SENB and SENT have been selected as fracture mechanics specimens herein to study the ductile fracture behavior of pipeline steels. Figure 2 shows the configurations of the edge-cracked specimens, where  $W$  ( $W = 12.7$  mm) is the specimen width,  $a$  is the crack depth, and  $2H$  is the weld width. The span ( $S$ ) of the SENB is molded as four times of specimen width ( $S/W = 4$ ) and  $2L/W = 10$  for SENT. The weld fracture specimen is modeled as a bi-material (weld metal and base metal), and the weld zone remains unchanged ( $2H \times W = 6$  mm  $\times$  12.7 mm) in all of the numerical analyses. Only a half specimen is modeled due to symmetry. Finite element calculations are performed while using two-dimensional (2D) plane strain models with four-node elements (ABAQUS: CPE4). Figure 2c shows the global mesh arrangement for all models. The region, 3.0 mm above the symmetrical interface, was uniformly meshed (0.1 mm  $\times$  0.1 mm) and it was used for the simulation of the ductile fracture process. Regarding to the ductile fracture on the basis of complete Gurson model, the element is assumed to damage fail by a specific judgement that the void volume fraction reaches a certain value  $f_F$  according to the relation  $f_F = 0.2 + 2f_0$  by UMAT in ABAQUS. The deformed elements appear along the damage layer in front of the crack tip. More details regarding the ductile fracture simulation model were presented in [38].

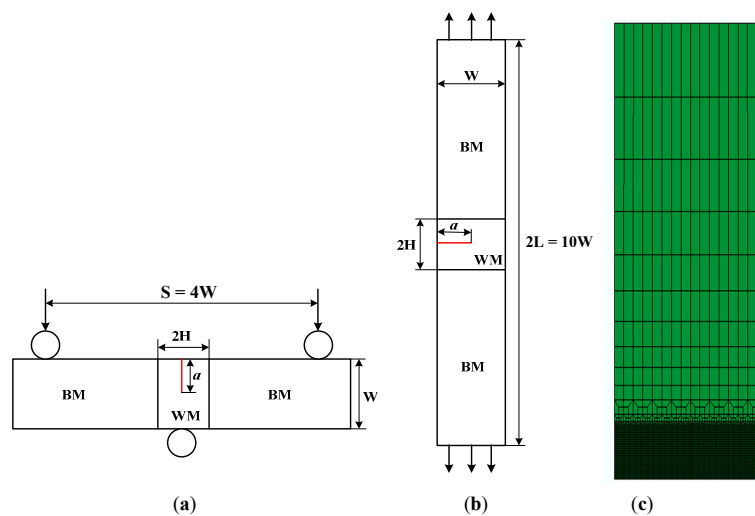


**Figure 2.** Schematic plots of the specimens, (a) single edge notched bending (SENB); (b) single edge notched tension (SENT); and, (c) finite element mesh.

### 2.4.2. Pipe

Figure 3a shows the geometry of only part of a pipe with an internal circumferential crack. Figure 3b displays the sketch of the axisymmetric pipe, in which  $2L$  is the pipe length,  $t$  is the pipe wall thickness,  $a$  is the crack depth,  $D$  is outer diameter, and  $H = 3$  mm is the half width of the weld. The same finite element mesh as 2D plane strain models is built in the axisymmetric model. In all the analyses, the pipe wall thickness is fixed to  $t = W = 12.7$  mm,  $D/W = 32$ , and  $L/t = 5$ . Still only half of pipe was modeled according to the symmetry. 2D axisymmetric models employ four-node elements (ABAQUS: CAX4) are used for the numerical study.

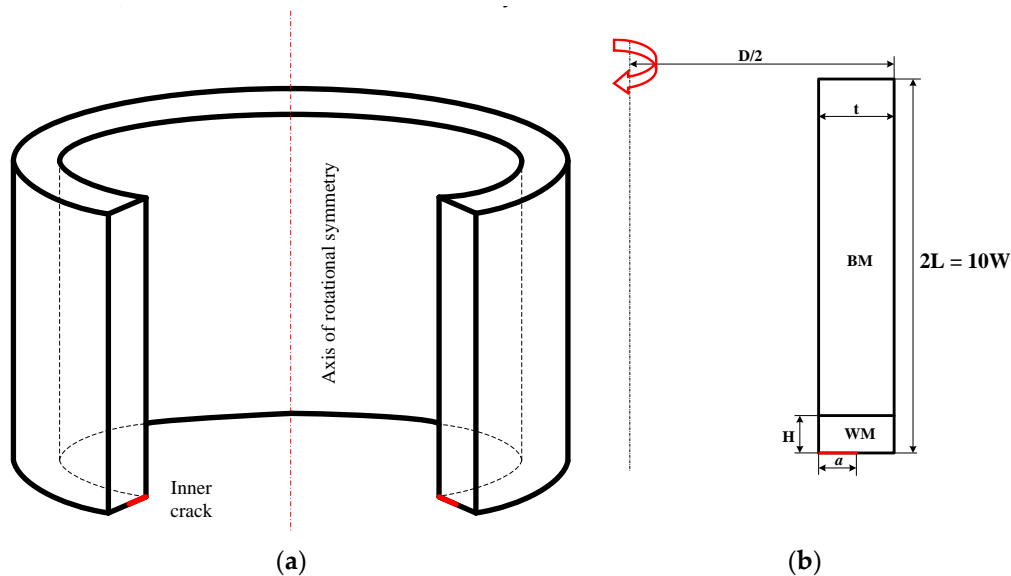


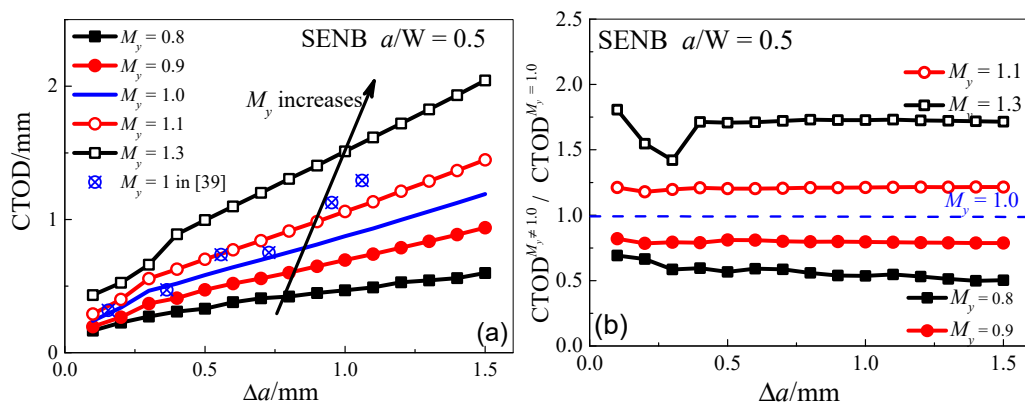
**Figure 3.** Schematic plots of pipe, (a) inner-cracked pipe; (b) schematic illustration of axisymmetric model.

## 3. Results and Discussion

This section provides the numerical results that were obtained from SENB, SENT, and cracked pipes in detail. The CTOD, extracted from the displacement of node in front of the initial crack tip, is chosen as the fracture parameter to describe the crack growth resistance and the crack driving force in all of the analyses.

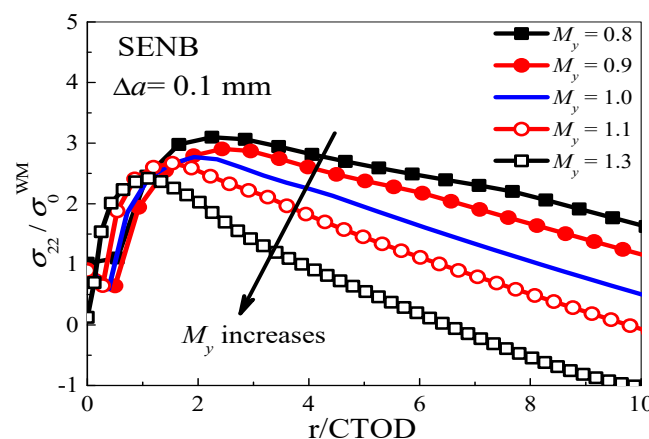
### 3.1. SENB

Figure 4a shows the crack growth resistance curves for the standard SENB specimen ( $a/W = 0.5$ ) with different strength mismatch levels. A strong effect of weld strength mismatch on the initial fracture toughness and dynamic fracture toughness can be clearly seen. The resistance curves significantly increase with the increase of strength mismatch levels (from  $M_y = 0.8$  to  $M_y = 1.3$ ). A similar result was also found in Ref. [39]. The related experimental data (Blue points) from [40] have been used to compare the Finite Element Method (FEM) results for the case of evenmatched ( $M_y = 1$ )  $a/W = 0.5$  SENB specimens. It is observed that the comparison exhibits, good agreement in the range of  $\Delta a = 0.75$ , while it exerts a slight deviation above this value. It can be attributed to the discrepancy of material property. These results further validate the effectiveness of the FEM model. Figure 4b shows the normalized crack growth resistance ( $CTOD^{M_y \neq 1.0}/CTOD^{M_y = 1.0}$ ), e.g., the resistance curves for  $M_y \neq 1.0$  were normalized by the resistance curves for  $M_y = 1.0$ . The dash line without marker indicates the case for  $M_y = 1.0$ . It is obvious to see that the effect of the strength mismatch on resistance curve tends to be less relevant to the amount of crack extension.



**Figure 4.** Effect of strength mismatch on crack growth resistance, (a) ductile resistance curves; (b) normalized crack growth resistance curves.

The opening stress distributions in front of the crack tip for all the mismatched specimens at  $\Delta a = 0.1$  mm are charted in Figure 5 to better understand the effect of strength mismatch on the ductile tearing resistance curves for SENB specimens. It shows that the opening stress for different mismatched cases expressed a gradually lower peak value with the increases of  $M_y$  at the same crack growth, therefore yields the increasingly higher resistance curve, as shown above in Figure 4a. It can also be seen that, with the increase of distance from crack tip, the crack opening stress rapidly declines, and then transforms into compressive stress, which could be influenced by the remote field [40,41].



**Figure 5.** The distribution of crack tip opening stress ahead of the crack tip at  $\Delta a = 0.5$  mm for different mismatched SENB specimens.

The equivalent plastic strain ( $\epsilon_p$ ) ahead of the current crack tip for all the mismatched SENB specimens at  $\Delta a = 0.1, 0.5$  and  $1.5$  mm are also presented in Figure 6, respectively, for further understanding the effect of strength mismatch on resistance curves with crack growth. At crack initiation,  $\Delta a = 0.1$  mm, a comparatively small influence of  $M_y$  on the equivalent plastic strain can be observed. But still, a higher  $\epsilon_p$  for the mismatched SENB specimen can be expected for the case with a larger  $M_y$  (see Figure 6a). With further crack growth, e.g.,  $\Delta a = 0.5$  mm and  $1.5$  mm, a much more evident effect of mismatch ratio on the equivalent plastic strain can be seen for all of the mismatched SENB specimens. Moreover, the equivalent plastic strain significantly increases with the increase of strength mismatch ratios, which again well explains the increasing resistance curves with increasing mismatch ratios, as observed in Figure 4a.

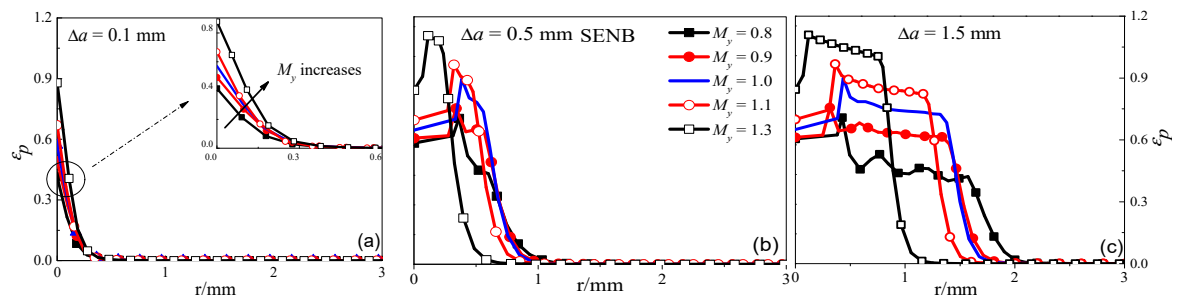


**Figure 6.** Equivalent plastic strain distributions ahead of the current crack tip for all the mismatched SENB specimens, (a)  $\Delta a = 0.1$  mm; (b)  $\Delta a = 0.5$  mm; and, (c)  $\Delta a = 1.5$  mm.

### 3.2. SENT

In this study, the SENT specimens with shallow ( $a/W = 0.2$ ) and deep ( $a/W = 0.5$ ) cracks are considered for comparison. Figure 7 shows the crack growth resistance curves for variously mismatched SENT specimens. It can be observed that the resistance curves significantly increase with the increase of strength mismatch levels for both shallow and deep-cracked SENT specimens, which is consistent with that of the SENB specimens. The normalized crack growth resistance curves ( $CTOD^{M_y \neq 1.0} / CTOD^{M_y = 1.0}$ ) were also studied, and similar results as that of SENB have been observed.

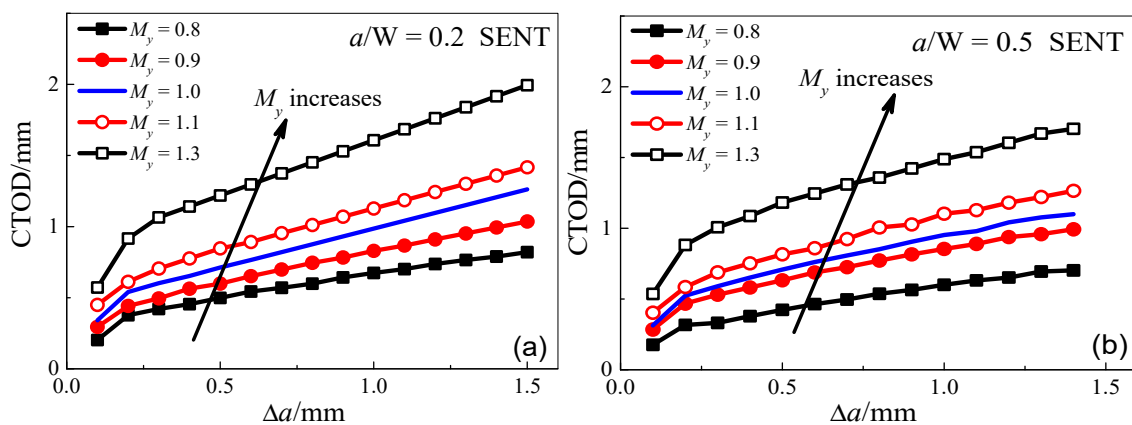


**Figure 7.** CTOD– $\Delta a$  curves for shallow- and deep-cracked SENT specimens with different mismatch ratios, (a)  $a/W = 0.2$ ; (b)  $a/W = 0.5$ .

Figure 8 presents the opening stress distributions in front of the current crack tip for the deep-cracked SENT ( $a/W = 0.5$ ) specimens at  $\Delta a = 0.1$  mm,  $0.5$  mm, and  $1.0$  mm in order to further understand the effect of strength mismatch on resistance curves with crack growth. It can be seen that, at certain crack growth ( $\Delta a = 0.1$  mm,  $0.5$  mm, and  $1.0$  mm), the peak stress obviously increases with the decrease of strength mismatch level  $M_y$ , which could therefore well explain the increased resistance curves with the increase of  $M_y$ , as depicted in Figure 7b. Additionally, similar observations have also been obtained for the shallow-cracked SENT specimens ( $a/W = 0.2$ ) with different mismatch ratios and, for the sake of simplicity, the results are not included here.



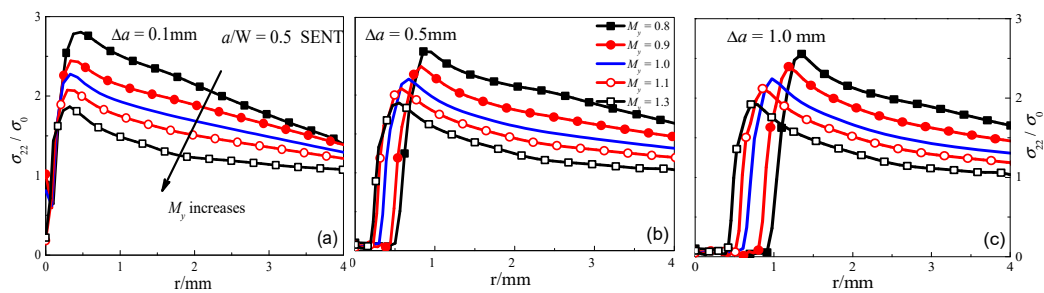


**Figure 8.** Crack tip opening stress distributions ahead of current crack tip,  $a/W = 0.5$ , (a)  $\Delta a = 0.1$  mm; (b)  $\Delta a = 0.5$  mm; (c)  $\Delta a = 1.0$  mm.

### 3.3. Pipe

In this subsection, finite element analyses for circumferentially cracked pipes with full internal cracks having two different  $a/t$  ratios ( $a/t = 0.2$  and  $0.5$ ) are conducted. Figure 9 displays the ductile fracture resistance curves for pipes with different mismatch ratios. It can be seen that, throughout the crack growth process considered in this study, pipes with higher  $M_y$  yield remarkably higher resistance curves for both the shallow and the deep cracked cases, which is still consistent with that of the SENB and SENT specimens.

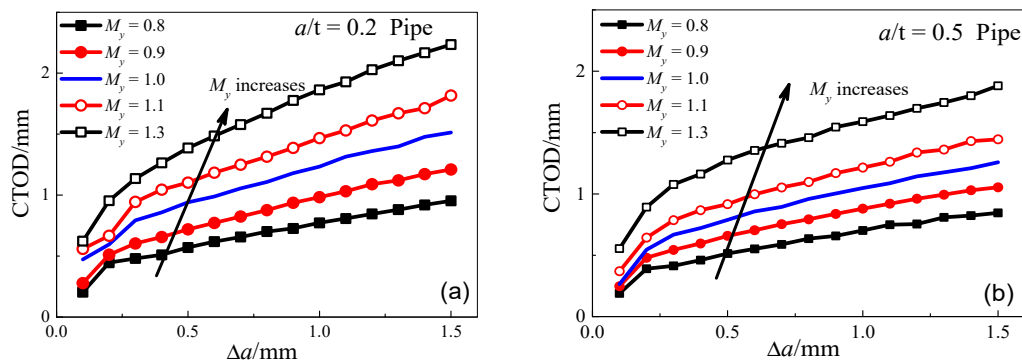


**Figure 9.** CTOD– $\Delta a$  curves for pipes with different mismatch ratios, (a)  $a/t = 0.2$ ; and, (b)  $a/t = 0.5$ .

The quantity of  $3\sigma_m/2\sigma_e$  (where  $\sigma_m$  and  $\sigma_e$  are the mean stress and effective stress, respectively) defines a convenient measure of triaxiality linked to the growth rate of micro-scale voids consistent with the subsequently introduced damage measures [42]. In the following, Figure 10 presents the stress triaxiality distributions along the ligament ahead of the current crack tip for shallow-cracked pipes ( $a/t = 0.2$ ) at different crack growth ( $\Delta a = 0.1$  mm,  $0.5$  mm, and  $1.0$  mm). What is interesting to observe is that the reduction of the stress triaxiality with the increase of  $M_y$  applies to the whole range of interest,  $0 < r < 8CTOD$ . At  $\Delta a = 0.1$  mm (see Figure 10a), the pipe with the highest mismatch ratio  $M_y$  exhibits the lowest stress triaxiality value, therefore producing the highest resistance curve, which corresponds to our above findings (see Figure 9a). For a propagating crack, the similar results can also be obtained, as shown in Figure 9b,c. Similar observations have also been obtained for the deep-cracked pipe ( $a/W = 0.5$ ) with different mismatch ratios, while the results are not included here in order to avoid repetition.

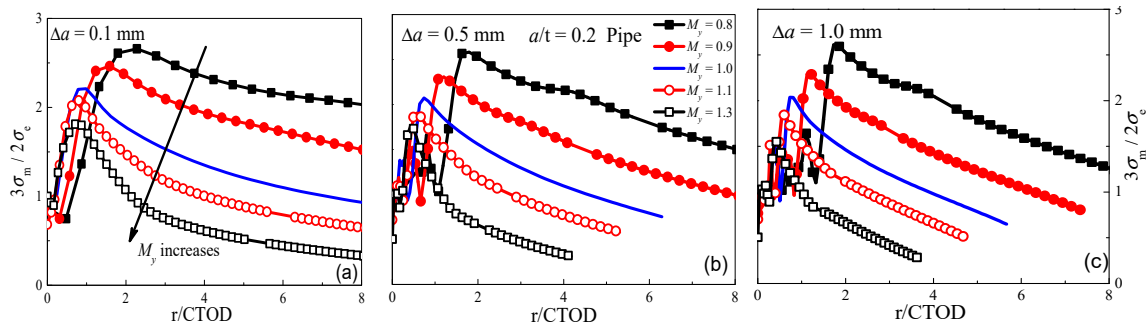


**Figure 10.** Stress triaxiality distributions ahead of the current crack tip for pipes at different crack propagation,  $a/t = 0.2$ , (a)  $\Delta a = 0.1$  mm; (b)  $\Delta a = 0.5$  mm; and, (c)  $\Delta a = 1.0$  mm.

### 3.4. Comparisons of Different Models

It has been shown that, in the elastic-plastic regime, the use of standard deeply notched SENB with crack depth of  $a/W = 0.5$  specimens provide a conservative assessment of fracture toughness for both weld metal and because of the high constraint that is associated with this specimen geometry. Use of specimen geometries and loading modes associated with lower constraint (e.g., SENT specimens), allow for improved estimates of fracture toughness to be made that are appropriate for the assessment of circumferential flaws in pipe girth welds. The resistance curves of all the models mentioned above are plotted together in Figure 11. Three different mismatched cases from under-match to even-match and over-match are considered herein for comparison. A minor influence of geometric models on the crack initiation toughness can be found for all these three mismatched cases. With the increase of  $M_y$  (e.g.,  $M_y = 1.0$  and  $1.3$ ), the difference in resistance curves for pipes ( $a/t = 0.2, 0.5$ ) and the corresponding SENT specimens (same crack depth, e.g.,  $a/W = 0.2, 0.5$ ) tends to be distinct. It can also be seen that the results from SENB specimen is obviously more conservative than that from SENT with respect to the pipes for all three mismatched cases considered in this study, which therefore can validate that the SENT specimen is a good representation of circumferentially cracked pipes for the fracture mechanics testing in engineering critical assessment and an alternative to the conventional standard SENB specimen, similar findings have also been discussed for circumferentially cracked pipes, as can be seen in reference [17].

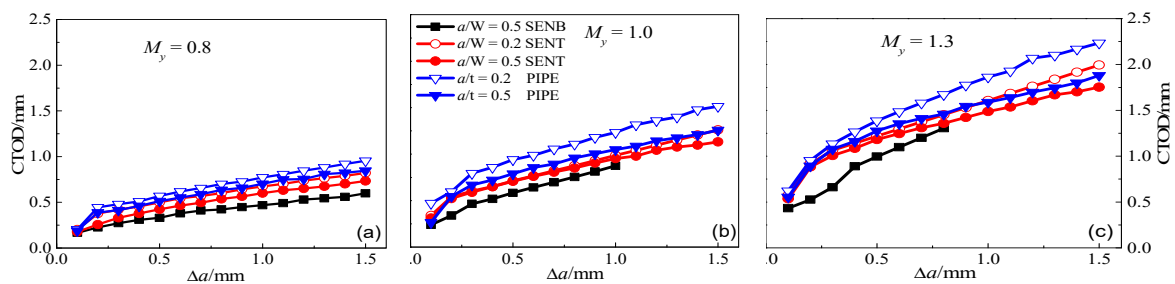


**Figure 11.** Comparisons of resistance curves for SENB, SENT and pipe, (a)  $M_y = 0.8$ ; (b)  $M_y = 1.0$ ; and, (c)  $M_y = 1.3$ .

### 3.5. Strength Mismatch Constraint Ahead of a Growing Crack

In this subsection, a so-called CTOD-Q-M formulation was proposed to describe the near-tip stress field in the presence of both geometry and mismatch constraints, in which the Q parameter describes the geometry constraint and the M value is used to rank the mismatch effect on the crack tip constraint.

The finite element analysis results have shown that the strength mismatch applied to models after a crack will induce an additional crack tip constraint. The mismatch constraint parameter M of SENT and pipe versus CTOD is calculated by Equation (6) and respectively plotted in Figure 12. The mismatch constraint M transforms from positive to negative with the increase of mismatch ratio

for the mismatched specimens with the same crack growth, unlike the geometry-induced crack tip constraint  $Q$ -parameter that is usually negative and decreases with the plastic deformation, which can further explain the effect of strength mismatch on ductile fracture behavior. Additionally, with crack growth, the value of  $M$  varies in a similar range, which indicates the effect of the strength mismatch on resistance curves is not quite associated with the amount of crack extension. At the same mismatched ratios (e.g., under-match and over-match), the mismatch constraint parameter  $M$  for pipes are comparatively lower than that of the corresponding SENT specimen.

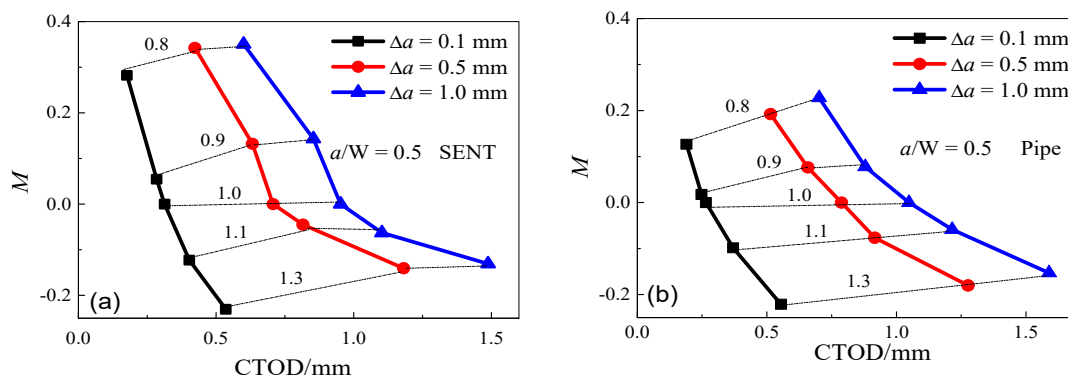


Figure 12.  $M$  versus CTOD for the mismatched specimens (a) SENT; (b) pipe.

#### 4. Conclusions

In accordance with the results presented, the following conclusions may be drawn:

- (1) Weld strength mismatch ratio shows a strong effect on the fracture toughness and ductile crack growth resistance curves for welding pipes. With the increase of mismatch ratio, the ductile fracture resistances significantly increase for the standard SENB and the shallow and deep-cracked pipes, as well as the corresponding SENT specimens.
- (2) For all of different mismatched cases considered in this study, the ductile tearing resistance from SENB specimen is obviously conservative than that from SENT with respect to the pipes, which can therefore validate that the SENT specimen is a good representation of pipes with circumferential cracks and an alternative to the conventional standard SENB specimen for the fracture mechanics testing in engineering critical assessment of strength-mismatched welding pipes.
- (3) The mismatch constraint  $M$  decreases from positive to negative with the increase of mismatch ratio ( $M_y = 0.8 \sim 1.3$ ) as for pipes and the corresponding SENT specimens. In addition, the mismatch constraint parameter  $M$  for pipes is comparatively lower than that of the corresponding SENT specimen at the same mismatched ratios.

**Author Contributions:** Investigation, Methodology and Calculations, L.S.; Revision, L.C.; Supervision, J.X., W.S. and F.B.; Writing—original draft, P.L.; Writing—review & editing, H.G. All authors have read and agreed to the published version of the manuscript.

**Funding:** This research was funded by National Natural Science Foundation of China (Project No. 51301197) and the Natural Science Foundation of Jiangsu Province (Project No. BK20130182) and the Fundamental Research Funds for the Central University (Project No. 2011QNA07) as well as the National Key R&D Program of China (2018YFB2001200).

**Acknowledgments:** Zhiliang Zhang from Norwegian University of Science and Technology is sincerely appreciated for his UMAT subroutine for the Complete Gurson Model and valuable comments.

**Conflicts of Interest:** The authors declare no conflict of interest.

## References

1. Garwood, S.J. *Effect of Specimen Geometry on Crack Growth Resistance, Fracture Mechanics*; ASTM STP 677; ASTM: Philadelphia, PA, USA, 1979.
2. Hancock, J.W.; Reuter, W.G.; Parks, D.M. *Constraint and Toughness Parameterized by T. Constraint Effects in Fracture*; ASTM STP 1171; ASTM: Philadelphia, PA, USA, 1993.
3. Donato, G.V.P.; Rebello, J.M.A.; Ruggieri, C. A two-parameter approach to assess effects of constraint in cracks located at geometrical discontinuities. *J. Strain Anal. Eng.* **2014**, *49*, 274–285. [[CrossRef](#)]
4. Betegon, C.; Hancock, J.W. Two-parameter characterization of elastic–plastic crack-tip fields. *J. Appl. Mech.* **1991**, *58*, 104–110. [[CrossRef](#)]
5. O’Dowd, N.P.; Shih, C.F. Family of crack-tip fields characterized by a triaxiality parameter: Part-I. Structure of fields. *J. Mech. Phys. Solids* **1991**, *39*, 989–1015. [[CrossRef](#)]
6. O’Dowd, N.P.; Shih, C.F. Family of crack-tip fields characterized by a triaxiality parameter-II. Fracture applications. *J. Mech. Phys. Solids* **1992**, *40*, 939–963. [[CrossRef](#)]
7. Nyhus, B.; Østby, E.; Thaulow, C.; Zhang, Z.L.; Olden, V. *SENT Testing and the Effect of Geometry Constraint in High Strength Steel*; International Symposium High Strength Steel: Trondheim, Norway, 2002.
8. Tyson, W.R.; Shen, G.; Roy, G. Effect of biaxial stress of ECA of pipelines under strain-based design. In Proceedings of the 17th International Offshore and Polar Engineering Conference, Lisbon, Portugal, 1–6 July 2007.
9. Cravero, S.; Ruggieri, C. Estimation procedure of J-resistance curves for SE(T) fracture specimens using unloading compliance. *Eng. Fract. Mech.* **2007**, *74*, 2735–2757. [[CrossRef](#)]
10. Xu, J.; Zhang, Z.L.; Østby, E. Constraint effect on the ductile crack growth resistance of circumferentially cracked pipes. *Eng. Fract. Mech.* **2010**, *77*, 671–684. [[CrossRef](#)]
11. Cray, M.J.; Luxmore, A.R.; Sumpter, J.D.G. The effect of weld metal mismatch on J and CTOD. In Proceedings of the European Symposium on Elastic-Plastic Fracture Mechanics, Freiburg, Germany, 9–12 October 1989.
12. Zhang, Z.L.; Thaulow, C.; Hauge, M. Effects of crack size and weld metal mismatch on the HAZ cleavage toughness of weld plates. *Eng. Fract. Mech.* **1997**, *57*, 653–664. [[CrossRef](#)]
13. Burstow, M.C.; Howard, I.C.; Ainsworth, R.A. The influence of constraint on crack tip stress fields in strength mismatched welded joints. *J. Mech. Phys. Solids* **1998**, *46*, 845–872. [[CrossRef](#)]
14. Zhang, Z.L.; Hauge, M.; Thaulow, C. Two-parameter characterization of the near-tip stress fields for a bi-material elastic–plastic interface crack. *Int. J. Fract.* **1996**, *79*, 65–83. [[CrossRef](#)]
15. Zhang, Z.L.; Hauge, M.; Thaulow, C. The effect of T stress on the near tip stress field of an elastic–plastic interface crack. In Proceedings of the Ninth International Congress on Fracture, Sydney, Australia, 1–5 April 1997.
16. Thaulow, C.; Hauge, M.; Zhang, Z.L.; Ranestad, Ø.; Fattorini, F. On the interrelationship between fracture toughness and material mismatch for cracks located at the fusion line of weldments. *Eng. Fract. Mech.* **1999**, *64*, 367–382. [[CrossRef](#)]
17. Ren, X.B.; Zhang, Z.L.; Nyhus, B. Effect of residual stresses on the crack-tip constraint in a modified boundary layer model. *Int. J. Solids Struct.* **2009**, *46*, 2629–2641. [[CrossRef](#)]
18. Zerbst, U. Application of fracture mechanics to welds with crack origin at the weld toe: A review Part 1: Consequences of inhomogeneous microstructure for materials testing and failure assessment. *Weld. World* **2019**, *63*, 1715–1732. [[CrossRef](#)]
19. Ruggieri, C. Further results in J and CTOD estimation procedures for SE(T) fracture specimens—Part I: Homogeneous materials. *Eng. Fract. Mech.* **2012**, *79*, 245–265. [[CrossRef](#)]
20. Paredes, M.; Ruggieri, C. Further results in J and CTOD estimation procedures for SE(T) fracture—Part II: Weld centerline cracks. *Eng. Fract. Mech.* **2012**, *89*, 24–39. [[CrossRef](#)]
21. Sarikka, T.; Ahonen, M.; Mougnot, R.; Nevasmaa, P.; Karjalainen-Roikonen, P.; Ehrnstén, U.; Hänninen, H. Effect of mechanical mismatch on fracture mechanical behavior of SA 508—Alloy 52 narrow gap dissimilar metal weld. *Int. J. Press. Vessel. Pip.* **2017**, *157*, 30–42. [[CrossRef](#)]
22. Sarikka, T.; Ahonen, M.; Mougnot, R.; Nevasmaa, P.; Karjalainen-Roikonen, P.; Ehrnstén, U.; Hänninen, H. Microstructural, mechanical, and fracture mechanical characterization of SA 508-Alloy 182 dissimilar metal weld in view of mismatch state. *Int. J. Press. Vessel. Pip.* **2016**, *145*, 13–22. [[CrossRef](#)]

23. Qiang, B.; Wang, X. Ductile crack growth behaviors at different locations of a weld joint for an X80 pipeline steel: A numerical investigation using GTN models. *Eng. Fract. Mech.* **2019**, *213*, 264–279. [[CrossRef](#)]
24. Gurson, A.L. Plastic Flow and Fracture behavior of Ductile Materials Incorporating Void Nucleation, Growth and Coalescence. Ph.D. Thesis, Brown University, Providence, RI, USA, 1975.
25. Tvergaard, V. Influence of voids on shear band instabilities under plane strain conditions. *Int. J. Fract.* **1981**, *17*, 389–407. [[CrossRef](#)]
26. Tvergaard, V. On localization in ductile materials containing spherical voids. *Int. J. Fract.* **1982**, *18*, 237–252.
27. Tvergaard, V.; Needleman, A. Analysis of the cup–corn fracture in a round tensile bar. *Acta Metall.* **1984**, *32*, 157–169. [[CrossRef](#)]
28. Thomason, P.F. *Ductile Fracture of Metals*; Pergamon Press: Oxford, UK, 1990.
29. Zhang, Z.L.; Thaulow, C.; Odegard, J. A complete Gurson model approach for ductile fracture. *Eng. Fract. Mech.* **2000**, *67*, 155–168. [[CrossRef](#)]
30. Zhang, Z.L.; Niemi, E. A class of generalized mid-point algorithms for Gurson-Tvergaard continuum damage material model. *Int. J. Numer. Meth. Eng.* **1995**, *88*, 2033–2053. [[CrossRef](#)]
31. Zhang, Z.L. On the accuracies of numerical integration algorithms for Gurson pressure-dependent elastoplastic constitutive models. *Comput. Meth. Appl. Mech. Eng.* **1995**, *121*, 15–28. [[CrossRef](#)]
32. Zhang, Z.L. Explicit consistent tangent moduli with a return mapping algorithm for pressure-dependent elastoplasticity models. *Comput. Meth. Appl. Mech. Eng.* **1995**, *121*, 29–44. [[CrossRef](#)]
33. Eikrem, P.A.; Zhang, Z.L.; Nyhus, B. Effect of plastic prestrain on the crack tip constraint of pipeline steels. *Int. J. Press. Vessel. Pip.* **2007**, *84*, 708–715. [[CrossRef](#)]
34. Liu, J.; Zhang, Z.L.; Nyhus, B. Residual stress induced crack tip constraint. *Eng. Fract. Mech.* **2008**, *75*, 4151–4166. [[CrossRef](#)]
35. Ren, X.B.; Akselsen, O.M.; Nyhus, B. Influence of welding residual stresses on the ductile crack growth resistance of circumferentially cracked pipe. *Front. Struct. Civ. Eng.* **2012**, *6*, 217–223. [[CrossRef](#)]
36. Chao, Y.J.; Yang, S.; Sutton, M.A. On the fracture of solids characterized by one or two parameters: Theory and practice. *J. Mech. Phys. Solids* **1994**, *42*, 629–647. [[CrossRef](#)]
37. Shih, C.F. Relationship between the J-integral and the crack opening displacement for stationary and extending cracks. *J. Mech. Phys. Solids* **1981**, *29*, 305–326. [[CrossRef](#)]
38. Xu, J.; Zhang, Z.L.; Østby, E.; Nyhus, B.; Sun, D.B. Effect of crack depth and specimen size on ductile crack growth of SENT and SENB specimens for fracture mechanics evaluation of pipeline steels. *Int. J. Press. Vessel. Pip.* **2009**, *86*, 787–797. [[CrossRef](#)]
39. Jing, H.Y.; Zhu, Z.Q.; Huo, L.X. Effect of strength mismatching on fracture behavior for nuclear pressure vessel steel A508-III welded joints. *Trans. China Weld. Inst.* **2002**, *23*, 35–37.
40. Nyhus, B.; Østby, E.; Knagenhjelm, H.O.; Black, S.; Røstadsand, P.A. Experimental studies on the effect of crack length and asymmetric geometries on the ductile tearing resistance. In Proceedings of the OMAE2005, the 24th International Conference on Offshore Mechanics and Arctic Engineering, Halkidiki, Greece, 12–17 June 2005.
41. Zhu, X.K.; Leis, B.N. Bending modified J–Q theory and crack-tip constraint quantification. *Eng. Fract. Mech.* **2006**, *141*, 115–134. [[CrossRef](#)]
42. Sobotka, J.C.; Dodds, R.H.; Sofronis, P. Effects of hydrogen on steady, ductile crack growth: Computational studies. *Int. J. Solids Struct.* **2009**, *46*, 4095–4106. [[CrossRef](#)]

